

Structural and magnetic properties of a mechanochemically activated Ti-Fe₂O₃ solid mixture

A.A. Cristóbal¹, C.P. Ramos.^{2,5}, P.G. Bercoff^{3,5}, S. Conconi⁴, E.F. Aglietti⁴, P.M. Botta¹ and J. M. Porto López¹

¹ Instituto de Investigaciones en Ciencia y Tecnología de Materiales (INTEMA), CONICET-UNMdP, J.B. Justo 4302 - B7608FDQ - Mar del Plata, Argentina.

² Centro Atómico Constituyentes (CAC), CNEA, Av. Gral. Paz 1499 (1650). San Martín, Argentina

³ Facultad de Matemática, Astronomía y Física (FaMAF), Universidad Nacional de Córdoba, Medina Allende s/n, Ciudad Universitaria. (5000) Córdoba, Argentina.

⁴ Centro de Tecnología de Recursos Minerales y Cerámica (CETMIC), CONICET- CIC, Camino P. Centenario y 506 - B1897ZCA - M.B. Gonnet, Argentina.

⁵ Consejo Nacional de Investigaciones Científicas y Técnicas (CONICET).

Abstract

The mechanochemical effects on the reactivity and properties of a titanium/hematite powder mixture with molar ratio of 1/2 are investigated. Crystalline-phase structure, composition, hyperfine and magnetic behaviors were analyzed as a function of activation time by means of X-ray diffraction, scanning electron microscopy, Mössbauer spectroscopy and vibrating sample magnetometry. The results showed that at relatively short activation times metallic Ti reduces part of the ferric ions, yielding a complex product formed mainly by a mix of two solid solutions Fe_{3-x}Ti_xO₄ (titanomagnetites), both with very different x values (0 < x < 1). Also metallic iron and superparamagnetic hematite particles were detected by Mössbauer spectroscopy. As the mechanical treatment extends the composition of the reactive mixture changes, prevailing in the end the solid solution with higher x value. In contrast, when these activated samples are thermally treated the fraction of the solid solution which is richer in Ti diminishes. This fact produces a significant variation of the saturation magnetization of the obtained material.

Keywords: A. oxides, C. Mössbauer spectroscopy, X-ray diffraction, D. magnetic properties.

1. Introduction

Spinel ferrites of general formula Fe_{3-x}M_xO₄, where 0 < x < 1 and M is a transition-metal ion such as Mn, Zn, Cr, V, Cu, or Ti have drawn considerable attention in the last decades [1]. Partial substitution of Fe by these cations leads to the formation of solid solutions with magnetic properties crucially dependent on the electronic structure of the dopant and its distribution into the sites of the spinel crystal structure [2].

In the so-called titanomagnetites, Ti⁴⁺ ions occupy B (octahedral) sites, replacing part of Fe²⁺ ions. These compounds have been the subject of numerous experimental and theoretical investigations due to the interest they have awakened for Earth Science and Technology [3]. All the previous literature reports that Ti⁴⁺ ions reside on B sites but the location of the remaining Fe²⁺ cations is still controversial [4-7]. The end members of the series, Fe₃O₄ (x = 0, magnetite) and Fe₂TiO₄ (x = 1, ulvöspinel), are ferrimagnetic and antiferromagnetic oxides with Néel temperatures of 858 and 120 K, respectively [8-9].

Rocks contain micrometric as well as nanometric inclusions of natural titanomagnetites. The magnetic study of these oxides could help to increase the knowledge on the history of Earth [10]. These natural ferrites have a Ti atomic concentration close to 0.5 [11], adding an extra interest to the study of half-doped compositions. In this way, the synthetic titanomagnetite series Fe_{3-x}Ti_xO₄ (0 < x < 1) provides an excellent system for studying the evolution of magnetic and structural properties with titanium concentration. Several synthesis methods have been used to

prepare these oxides, such as solid-state reaction [6] under very low oxygen pressures and mechanochemical activation [12], both using stoichiometric mixtures of Fe, Fe₂O₃ and TiO₂. More recently, some soft-chemistry methods have been also employed in order to prepare nanocrystalline titanomagnetites [13].

It has been demonstrated that mechanochemical activation of inorganic solids is a useful tool for the preparation of metastable crystalline and amorphous phases, and also for nanostructured materials not-obtainable through conventional methods [14-16]. Some of the advantages of this method are shortening of reaction times, reduction of the high temperatures commonly required for solid-state reactions and the possibility of producing materials with special properties [17]. The high concentration of lattice defects introduced by the mechanical treatment often produces phases with distorted crystalline structures and modified cation distributions. This characteristic has been profited for preparing several transition metal oxides with special properties (ferrimagnetic spinels, ferro and piezoelectric perovskites, etc.) [18-20].

In this work, continuing a series of previous studies [21,22], we have investigated the mechanochemical activation of a Ti/Fe₂O₃ mixture with a molar ratio of 1/2. The use of metallic Ti is an interesting alternative since for other mechanoactivated metal-oxide systems the formation of precursors in relatively mild conditions, or even the ignition of self-sustained reactions close to room temperature have been reported [23,24].

Phase evolution, structural features, hyperfine properties and magnetic response of the solid mixture are analyzed as a function of activation time using information provided by X-ray diffraction (XRD), scanning electron microscopy (SEM), Mössbauer spectroscopy (MS) and vibrating sample magnetometry (VSM).

2. Experimental

2.1 Preparation of samples

The reactive mixture was prepared from 98 wt.% metallic Ti and 99 wt.% hematite, both commercial reagents. The average particle size of both reactants was 20 and 5 μm for Ti and hematite respectively. The initial mixture Ti/Fe₂O₃ –with molar ratio 1/2– was activated in a laboratory planetary ball-mill (Fritsch Pulverisette 7) with vials and balls of hardened Cr-steel.

The mixture was prepared and activated under Ar atmosphere ($P_{\text{oxygen}} < 1 \text{ Pa}$). The experimental method assured there was no leaking of oxygen from the outer atmosphere into the vials. The milling bowls were loaded with 5 g of powder and 7 balls of 15 mm diameter each, resulting in a ball-to-powder mass ratio of 20:1, and they were rotated at 1500 rpm during measured times. The obtained samples were labelled TiHx, where x is the activation time in hours.

A thermal treatment at 700°C was then performed on the powders under an Ar flow using a heating rate of 10°C min⁻¹, and a soaking time of 30 min at the final temperature (samples TiHx-700).

2.2 Analysis and characterization of samples

Crystalline phases were characterized by XRD with a Philips 3020 Goniometer with PW 3710 controller, Cu-Kα radiation and Ni filter at 40 kV and 20 mA. The scanning was done between 15° and 65° in 2θ with step counting time of 4 seconds. Silicon powder was added to all the samples as an internal reference. Powder diffraction patterns were analyzed with FullProf [25], a multipurpose profile-fitting program including Rietveld refinement. The starting crystallographic data for each phase were extracted from the literature [26-30].

Particle morphology and size of the activated samples were examined by SEM (Philips 505).

Mössbauer spectra were taken at room temperature (RT) in a conventional constant acceleration spectrometer in transmission geometry with a ⁵⁷Co/Rh source. The absorber thickness

was chosen to be the optimum according to the Long et al. criterion [31]. Spectra were fitted by using the Normos program [32].

Magnetic measurements were performed on the samples at room temperature using a Vibrating Sample Magnetometer Lakeshore 7300. The powders were shaped into disks of 6 mm diameter and 1 mm height and compacted with the aid of a uniaxial press using 5 Tons. Hysteresis loops were obtained varying the applied field between ± 15 kOe.

3. Results and Discussion

XRD patterns of the TiHx series of samples are shown in Figure 1. A decrease of the diffracted intensities for Ti and hematite is observed together with a widening of the peaks when the activation time increases (Fig. 1a). This broadening is due to the decrease of the crystal size and the disordering of the crystalline structure provoked by the mechanical treatment. These peaks completely disappear after 3 h of activation. At this time the formation of a crystalline phase corresponding to a spinel structure is observed. These peaks were attributed to titanomagnetite ($\text{Fe}_{3-x}\text{Ti}_x\text{O}_4$) with an uncertain Ti concentration. In addition, metallic iron ($\alpha\text{-Fe}$) became visible from 2h of milling time (main peak at $2\theta \sim 44.6^\circ$). When these diffractograms were refined using the Rietveld method a poorly crystalline structure compatible with FeO was also identified.

The analysis of XRD measurements indicates that with increasing activation times, the rhombohedral structure of hematite changes to the titanomagnetite cubic structure. This is due to the progressive disordering of the hematite structure provoked by the mechanical treatment and also to the incorporation of Ti in its lattice.

The distortion of hematite structure together with the reduction of part of Fe^{3+} ions lead to the formation of a cubic spinel structure, where Ti^{4+} ions are gradually incorporated. This effect is supported by the variation of the lattice parameter a (estimated by using the Rietveld method), shown in Table 1. It is worth noting that the a value tends to the ulvöspinel lattice parameter ($a = 8.5352 \text{ \AA}$) [33] with increasing activation time, indicating that titanomagnetite has a higher Ti concentration (x value) for longer activation times.

Table 1. Lattice parameter (a) corresponding to $\text{Fe}_{3-x}\text{M}_x\text{O}_4$ spinel-phase calculated for samples TiH1, TiH2, TiH3 and TiH3700. Values in parenthesis represent estimated standard deviations in the last quoted place.

Sample	a (Å)	
TiH1	8.399(1)	
TiH2	8.433(1)	
TiH3	8.494(2)	
TiH3-700	Phase 1 8.389(1)	Phase 2 8.477(1)

Figure 1b shows XRD patterns for activated and heated samples. A comparison with the as-milled samples reveals that thermal treatment favoured the formation of titanomagnetite. The inset shows a detailed view of the main peak of this phase, which is in fact the result of the overlapping of two signals. These could be assigned to the formation of two solid solutions, one with x (Ti content) closer to 1 (peak centered on $35.1^\circ 2\theta$) and the other one with x closer to 0 (peak centered about $35.4^\circ 2\theta$). The relative fractions of these solid solutions change with activation time, increasing the amount of the Ti-richer spinel. For sample TiH3-700 both signals could be satisfactorily resolved and the lattice parameters obtained for each solid solution are shown in Table 1. Besides, the crystallite size was obtained for the spinel phase from the FWHM,

resulting in $270 \pm 7 \text{ \AA}$ for both compositions. On the other hand, peaks of ilmenite (FeTiO_3), with lower intensity for the samples activated during longer times, can be observed. Taking into account that ilmenite and hematite form a continuous series of solid solutions [8], the appearance of this mixed oxide could be the result of the partial substitution of Fe^{3+} by Ti^{4+} ions in remaining hematite (present in TiH1 and TiH2) when the activated solids are thermally treated. Moreover, the peaks corresponding to metallic Fe are more intense than those observed for the as-milled samples. However, this does not necessarily denote that the quantity of α -Fe increased. In the early stages of activation, the α -Fe (resultant from the redox reaction with Ti) -being in small clusters- could not be easily detectable by XRD [22]. Maybe at longer activation times and/or after thermal treatment, these domains became ordered and their diffracted intensity increased as a consequence.

Scanning electron micrographs of activated powders show that after three hours of activation (sample TiH3), the solid consists in agglomerates smaller than $40 \mu\text{m}$ in diameter (see inset, Figure 2a). These agglomerates are formed by rounded and poorly crystalline sub-micrometric particles with a relatively fine and homogeneous microstructure (Figure 2a). This considerable tendency to agglomeration is due not only to the small particle size caused by the milling process, but also to the high surface energy resulting from the high concentration of structural defects provoked by the activation. Figure 2b shows the microstructure of the TiH3-700 sample. Neither significant change in morphology nor in growth of particle size is observed (Figure 2b).

Mössbauer spectra of the TiH_x -700 samples (Figure 3) were acquired at RT and then computer-fitted using sextets and quadrupole-split doublets in most of the cases, hyperfine field distributions were added when was necessary. In the case of TiH2-700 and TiH3-700 a hyperfine field distribution was added to take into account hyperfine field values between ~ 12 and 30 T present in those spectra.

Table 2 displays the relative abundances of each Fe-bearing compound present in the samples. In the whole series the presence of hematite (H) is evident, with its characteristic hyperfine parameters ($B_{\text{hf}} \sim 51 \text{ T}$, $\text{IS} \sim 0.33 \text{ mm/s}$ and $\text{QS} \sim -0.20 \text{ mm/s}$) [34], and also titanomagnetite (T-M) can be detected, whose Mössbauer spectrum could be resolved by three sextets [35]. Two of them ($B_{\text{hf}} \sim 48$, $\text{IS} \sim 0.28 \text{ mm/s}$ and $B_{\text{hf}} \sim 45 \text{ T}$, $\text{IS} \sim 0.53 \text{ mm/s}$) correspond to Fe^{3+} and $\text{Fe}^{2.5+}$ on tetrahedral and octahedral sites of magnetite and an extra one ($B_{\text{hf}} \sim 41 \text{ T}$, $\text{IS} \sim 0.62 \text{ mm/s}$) appears as Ti substitutes Fe in the octahedral sites of the magnetite lattice.

Table 2. Relative abundancies of Fe-bearing phases obtained by Mössbauer analyses. H: hematite, T-M: titanomagnetite, α -Fe: Iron, sH: superparamagnetic hematite, n-sU: non-stoichiometric ulvöspinel, gp: grain-boundary phases.

Sample	H	T-M	α Fe	sH	n-sU	gp
TiH1	42	29	-	7	22	-
TiH2	9	20	5	14	52	-
TiH3	$\ll 1$	$\ll 1$	2	14	84	-
TiH1-700	26	48	6	8	12	-
TiH2-700	18	17	4	8	39	14
TiH3-700	6	10	7	5	54	18

The presence of α -Fe in all the samples except TiH1 is supported by the appearance of a sextet with a hyperfine magnetic splitting of 33 T . Its relative abundance shows a maximum of about 7% for TiH3-700. Spectra also reveal a main quadrupole doublet representative of Fe^{2+} species with $\text{QS} \sim 1.54 \text{ mm/s}$ and $\text{IS} \sim 0.94 \text{ mm/s}$. These hyperfine parameters are close to those of the stoichiometric ulvöspinel [36], then this doublet was assigned to “non-stoichiometric ulvöspinel” (n-sU) or a titanomagnetite with higher Ti content. It is interesting to note that the hyperfine parameters become closer to the stoichiometric values with increasing activation time for the heat-treated samples (for TiH3-700 the QS amounts to 1.73 mm/s and the IS to 0.94

mm/s). In the values of relative abundance given for n-sU (Table 2) a minor contribution of FeO and FeTiO₃ (both detected by XRD) cannot be disregarded.

The existence of both solid solutions with different Ti content (TM and n-sU) was also deduced from XRD results, but only for calcined samples since for the as-milled ones the crystallinity of the structures is very poor. It is then possible to estimate the Ti content in TiH3, because only one spinel phase is present in this sample. By using the lattice parameter calculated from the corresponding XRD pattern and applying Tanaka's results [35] it could be said that Ti content is near 0.6. This confirms that although the Ti global content is 0.5, there exist two spinel phases, one with a Ti content lower than 0.5 (T-M) and the other one with a higher Ti content (n-sU).

An additional quadrupole doublet (QS ~ 0.67 mm/s, IS ~ 0.32 mm/s) due to ferric iron with a low relative abundance was ascribed to superparamagnetic particles formed from bulk hematite as a consequence of the ball-milling process (sH). This assignment is not straightforward because there are various compounds which have very similar hyperfine parameters in that range but, finally, it could be done owing to a measurement at 15 K. These results were recently published elsewhere [22]. Comparing the spectra at RT and 15 K the magnetic transition distinctive of hematite could be detected, showing that the area covered by the quadrupole split doublet at RT was replaced by the characteristic hematite sextet at 15 K. This fact let us conclude that there is a distribution of particle sizes due to ball-milling. The very small ones, having a few nanometers, give a superparamagnetic contribution while the others stay in the magnetically ordered state characterized by the typical hematite sextet at 15 K.

The hyperfine field distributions between ~ 12 and 30 T found in the Mössbauer fitting procedure of TiH2-700 and TiH3-700 may arise from the development of disordered phases -due to the ball-milling process- which preferably locate on grain-boundaries. The fraction of these phases (gp) is also reported in Table 2 in terms of Fe content.

Examining the results shown in Table 2 for the as-milled samples, it follows that the main transformation consisting on the Fe³⁺ to Fe²⁺ reduction sets out before 1 h of milling the starting material. These results also indicate that after 3 h of activation crystalline hematite is almost completely reduced, except for the fraction of superparamagnetic hematite which remains untransformed. On the other hand, a decrease in the concentration of high-Ti content phase is observed together with an increase of the low-Ti content phase in the heat-treated powders compared to the corresponding as-milled ones. This fact indicates that during thermal treatment at 700°C oxidation of Fe²⁺ to Fe³⁺ is occurring, which leads to an increase in the spinel phase with higher concentration of ferric ions (T-M) at the expense of n-sU phase, richer in Fe²⁺ ions.

The evolution of the fractions of the main non-metallic Fe-bearing phases involved in the reduction process (Table 2) as a function of milling time is shown in Figure 4 for the as-milled samples (dot-lines are only a guide to the eye). In order to summarize the chemical changes occurring in the activated solid-state reaction, three different processes can be distinguished during the course of the iron reduction by titanium. The first one is associated with the continuous consumption of hematite, as ferric starting reactant. On the other hand, the fraction of non-stoichiometric ulvöspinel (high-Ti content titanomagnetite) monotonously increases, as a consequence of the reduction of part of ferric cations (hematite) to ferrous cations. Besides, from 2 h of activation time, the formation of this rich titanium phase is also fed by the reduction of ferric ions of titanomagnetite, whose fraction rises at the beginning of the activation but decreases for longer milling times. In summary, the scheme displays the complexity of a reactive system that evolves towards the formation of Fe_{3-x}Ti_xO₄, with increasing values of x as activation times increases.

Figure 5 shows the measured hysteresis loops of the as-milled samples and Table 3 contains the most relevant magnitudes derived from these curves for all the studied samples. The general tendency shows that saturation magnetization (Ms) is larger in the heat-treated samples than in the corresponding as-milled ones. This is because of the healing of both structural defects and damage produced during the milling to the different phases. Samples with better crystallinity are obtained after the thermal treatment and this results in more ordered structures with higher Ms.

Also, the increase of α -Fe in the heat-treated samples (see Table 2) is an important factor for larger Ms values.

Table 3. Coercivity (Hc), remanence (Mr) and saturation magnetization (Ms) of the studied samples.

Sample	Hc [Oe]	Mr [emu g ⁻¹]	Ms[emu g ⁻¹]
TiH1	340	2.6	17.0
TiH2	250	2.6	22.6
TiH3	220	1.7	10.2
TiH1-700	550	11.7	31.7
TiH2-700	580	6.9	22.7
TiH3-700	310	2.8	15.7

The value of Ms as a function of activation time first increases from 17.0 emu g⁻¹ (TiH1) to 22.6 emu g⁻¹ (TiH2) and then decreases to 10.2 emu g⁻¹ (TiH3). The increase in Ms is quite an unexpected behaviour since longer milling times are expected to produce more damaged structures and therefore smaller Ms values. In order to understand this behavior we should consider each sample composition and relative abundance of every phase. For this analysis we can disregard the presence of hematite since its Ms is around 0.8 emu g⁻¹ (see, for instance [37]) and its contribution to the total magnetization of these samples is negligible, or at the most it is within the measurement error. The phases which contribute to the total magnetization of the samples are α -Fe (being its saturation magnetization at room temperature as high as 219 emu g⁻¹ [38]) and the two spinel phases – the one with lower and the other with higher Ti content. According to Mössbauer results, TiH1 contains no α -Fe at all; however TiH2 does have ~ 5% of α -Fe. This fact and the marked increase of the high-Ti content phase (n-s U) in TiH2 with respect to TiH1 (see Table 2) are a reasonable explanation of the observed increase of Ms for t = 2 h. In contrast, even when the amount of the high-Ti content phase is as high as 84% in TiH3, the decrease of α -Fe to 2%, the vanishing of the low-Ti phase and the loss of crystallinity after 3 h of activation lead to a considerably lower Ms.

Coercivity –defined as the value of magnetic field for which magnetization is zero– is a macroscopic average of all the field-inversion processes occurring in the sample. In order to have a more precise and accurate insight of the demagnetization processes, magnetic susceptibility χ is often computed, since this magnitude is closely related to the inversion fields of the magnetic phases present in the samples. The observed peaks in χ vs H are associated to the distribution of inversion fields (the inversion field of a phase, denoted χ_{Hc} , is taken as the absolute value of the maximum of the corresponding peak in χ) and therefore provide useful information when studying samples with several interacting or non-interacting magnetic phases.

The curves χ vs H of our samples were obtained by calculating the derivative dM/dH of the superior branch of the corresponding hysteresis loop. The fitting of these curves was performed with the aid of the program PeakFit 4.12. The position of the peaks was determined with an error of about ± 20 Oe since displacements of this order of magnitude did not alter appreciably the regression coefficient. This was probably due to the dispersion of the experimental values.

The curves χ vs H for three selected samples are shown in Figure 6, together with their corresponding fits. At a first glance, one could be tempted to say that there is only one contribution to the susceptibility since there is a single apparent peak. However, a detailed analysis evidences that this is not true. From Mössbauer results on iron-bearing phases relative abundance (Table 2) we know that TiH1 does not contain α -Fe, so the susceptibility of this sample should be conformed by the superposition of three contributions: one from hematite (a peak centred around H=0 Oe), one from the low-Ti content titanomagnetite and the third one from the high-Ti content titanomagnetite. On the other hand, TiH3 has negligible amounts of T-M and

of hematite, so for this sample a peak centred on $H=0$ corresponding to α -Fe and another corresponding to n-s U are expected.

The calculated susceptibilities as well as the corresponding fits for TiH1 and TiH3 are shown in Figure 6 (top and middle panels, respectively). Even when their composition is quite different (refer to Table 2) these samples share common features in their susceptibilities – namely the peak at -500 Oe and the one centred at the origin. The last one is originated by hematite in TiH1 and by iron in TiH3. Since the only phase that is present both in TiH1 and in TiH3 is the high-Ti content titanomagnetite (n-s U), according to Table 2, we can conclude that the harder phase peak in χ corresponds to this phase. The softer phase peak observed in TiH1 at -210 Oe corresponds to the low-Ti content phase (T-M) which is not appreciably detected in TiH3.

It is worth remarking here the invariability of the inversion field observed for the n-sU phase in TiH1 and TiH3. This suggests that the composition of this phase in both samples would be very similar. In other words, two titanomagnetites with different Ti-contents are formed from 1 h of activation time, and ulterior milling only modifies the relative fractions of them without significantly changing their respective Ti-contents. Some differences in the shape of the peaks could be attributed to the different particle size distributions.

Sample TiH3-700 has a more complex magnetic structure considering that it contains many phases as well as grain boundary phases. In order to correctly fit the magnetic susceptibility of TiH3-700 four different peaks were needed (see Figure 6, bottom panel). The peaks corresponding to the soft phases centred on 0 Oe and the one at -500 Oe assigned to titanomagnetite with high-Ti content maintain their position with respect to the as-milled samples. However, the peak corresponding to the low-Ti content phase moves to lower nucleation fields (from -210 to -130 Oe), indicating that this phase has probably undergone a larger grain growth than the others, as a result of the heat-treatment. The appearance of a harder phase peak with nucleation fields around -1150 Oe could be attributed to the grain boundary phases detected by Mössbauer spectroscopy (see Table 2). However, the amount of these hard phases is not enough to considerably raise the coercivity (the macroscopic average of all the inversion fields) of this sample. In all the samples, some kind of magnetic interaction between the phases is present since the measured susceptibility consists of the convolution of the different contributions. The constant background in all the studied curves corresponds to a paramagnetic phase, probably superparamagnetic hematite which is present in all the samples.

4. Conclusions

The mechanochemical treatment of Ti/Fe₂O₃ solid mixtures produces several chemical reactions depending on the activation time. In the first hour, more than half of the initial hematite is consumed, emerging two solid solutions Fe_{3-x}Ti_xO₄ with different Ti contents. During the second hour the amount of hematite keeps on decreasing whereas a solid solution richer in Ti prevails over the other titanomagnetite. The formation of this high-Ti content phase is favoured during the final stage of the milling at the expenses of hematite and the low-Ti content phase, which are both nearly completely consumed. The presence of a small fraction of α -Fe is detected from 2 h, remaining almost constant for longer times and producing -at 2 h of activation time- the highest Ms value (22.6 emu g⁻¹) for the as-milled samples. Thermal treatments at 700°C favour the formation of the spinel phase with lower Ti-content leading to materials with higher Ms. In addition, TiH3-700 presents a hard magnetic phase with a nucleation field of -1150 Oe which is not abundant enough as to raise the coercivity of this sample.

There is also a paramagnetic contribution in all the studied samples (even in the heat-treated ones) which is attributed to the presence of superparamagnetic hematite, formed during the ball-milling process.

Acknowledgments

The authors thank CONICET, ANPCyT, UNMdP, SECyT-UNC and CNEA for the financial support given to this work.

References

- [1] M. Sugimoto, *J. Am. Ceram. Soc.* 82 (1999) 269-280.
- [2] J. Smit, H.P.J. Wijn, *Ferrites*, Wiley, Amsterdam, 1959.
- [3] E. Senderov, A. Dogan, A. Navrotsky, *Am. Mineral.* 78 (1993) 565–573.
- [4] Z. Kakol, J. Sabol, J.M. Honig, *Phys. Rev. B* 43 (1991) 649-654.
- [5] Z. Kakol, J. Sabol, J. Stickler, J.M. Honig, *Phys. Rev. B* 46 (1992) 1975-1978.
- [6] B. Wechsler, D. Lindsley, C. Prewitt, *Am. Mineral.* 69 (1984) 754–770.
- [7] G. Blasse, *Philips Res. Rep. Suppl.* 3 (1964).
- [8] R.M. Cornell, U. Schwertmann, *The iron oxides: Structure, Properties, Reactions, Occurrences and Uses*, Wiley-VCH, Weinheim, 2003.
- [9] A. Lyberatos, *J. Magn. Magn. Mater.* 311 (2007) 560-564.
- [10] B. M. Moskowitz, M. Jackson, C. Kissel, *Earth Planet. Sci. Lett.* 157 (1998) 141-149.
- [11] W.O' Reilly, *J. Magn. Magn. Mater.* 137 (1994) 167-185
- [12] F. Bernard, J. Lorimier, V. Nivoix, N. Millot, P. Perriat, B. Gillot, J.F. Berar, J.C. Niepce, *J. Solid State Chem.* 141 (1998) 105–113.
- [13] N. Guigue-Millot, Y. Champion, M.J. Hÿtch, F. Bernard, S. Bégin-Colin, P. Perriat, *J. Phys. Chem. B* (2001) 7125-7132.
- [14] K. Tkáčová, in: D.W. Fuerstenau (Ed.), *Developments in Mineral Processing*, vol. 11, Elsevier, Amsterdam, 1989.
- [15] C. Suryanarayana, *Prog. Mater. Sci.* 46 (2001) 1-184.
- [16] C. Suryanarayana, E. Ivanov, V.V. Boldyrev, *Mater. Sci. Eng. A* 304–306 (2001) 151-158.
- [17] D.L. Zhang, *Prog. Mater. Sci.* 49 (2004) 537-560.
- [18] B.H. Liu, J. Ding, Z.L. Dong, C.B. Boothroyd, J.H. Yin, J.B. Yi, *Phys. Rev. B* 74, (2006) 184427.
- [19] V. Šepelák, U. Steinike, D.Ch. Uecker, S. Wissmann, D. Becker, *J. Solid State Chem.* 135 (1998) 52-58.
- [20] M. Algueró, J. Ricote, T. Hungría, A. Castro, *Chem. Mater.* 19 (2007) 4982-4990.
- [21] A.A. Cristóbal, E.F. Aglietti, M.S. Conconi, J.M. Porto López, *Mater. Chem. Phys.* 111 (2008) 341–345
- [22] A.A. Cristóbal, C.P. Ramos, P.M. Botta, E.F. Aglietti, C. Saragovi, J.M. Porto López, *Physica B* 404 (2009) 2751-2753.
- [23] P.M. Botta, P. G. Bercoff, E. F. Aglietti, H. R. Bertorello and J. M. Porto López, *Mater. Eng. A* 360 (2003) 146-152.
- [24] L. Takacs, *Prog. Mater. Sci.* 47 (2002) 355–414.
- [25] J. Rodriguez-Carvajal "FULLPROF: A Program for Rietveld Refinement and Pattern Matching Analysis", *Abstracts of the Satellite Meeting on Powder Diffraction of the XV Congress of the IUCr* (1990) Toulouse, p. 127.
- [26] R.W.G. Wyckoff, *Crystal Structures*, Interscience Publishers, New York, 1963, p. 467.
- [27] R.J Hill, J.R. Craig, G.V. Gibbs, *Phys. Chem. Minerals* 4 (1979) 317-339.
- [28] R.L. Blake, R.E. Hessevick, *Am. Mineral.* 51 (1966) 123-129.
- [29] R.J. Harrison, S.A.T. Redfern, *Phys. Chem. Minerals* 28 (2001) 399-412.
- [30] B.A. Wechsler, D.H. Lindsley, C.T. Prewitt, *Am. Mineral.* 69 (1984) 754-770.
- [31] G.J. Long, T.E. Cranshaw, G. Longworth, *Mössbauer Effect Reference and Data Journal*, 6 (1983) 42.
- [32] R.A. Brand, *Normos program*, *Internat. Rep. Angewandte Physic*, Univ. Duisburg, 1987.
- [33] International Centre for Diffraction Data, File N° 34-0177.

- [34] R. E. Vandenberghe, Mössbauer spectroscopy and applications in geology, Apostilha International Training Centre for Post-Graduate Soil Scientists, 1991.
- [35] H. Tanaka, M. J. Kono, Geomag. Geoelectr. 39 (1987) 463-475.
- [36] M.D. Dyar, D.G. Agresti, M.W. Schaefer, C.A. Grant, E.C. Sklute, Annu. Rev. Earth Planet. Sci. 34 (2006) 83-125.
- [37] A. H. Morrish, Canted Antiferromagnetism: Hematite, World Scientific Publishing Co., Singapore, 1994.
- [38] R.M. Bozort, Ferromagnetism, IEEE Press, New York, 1993.

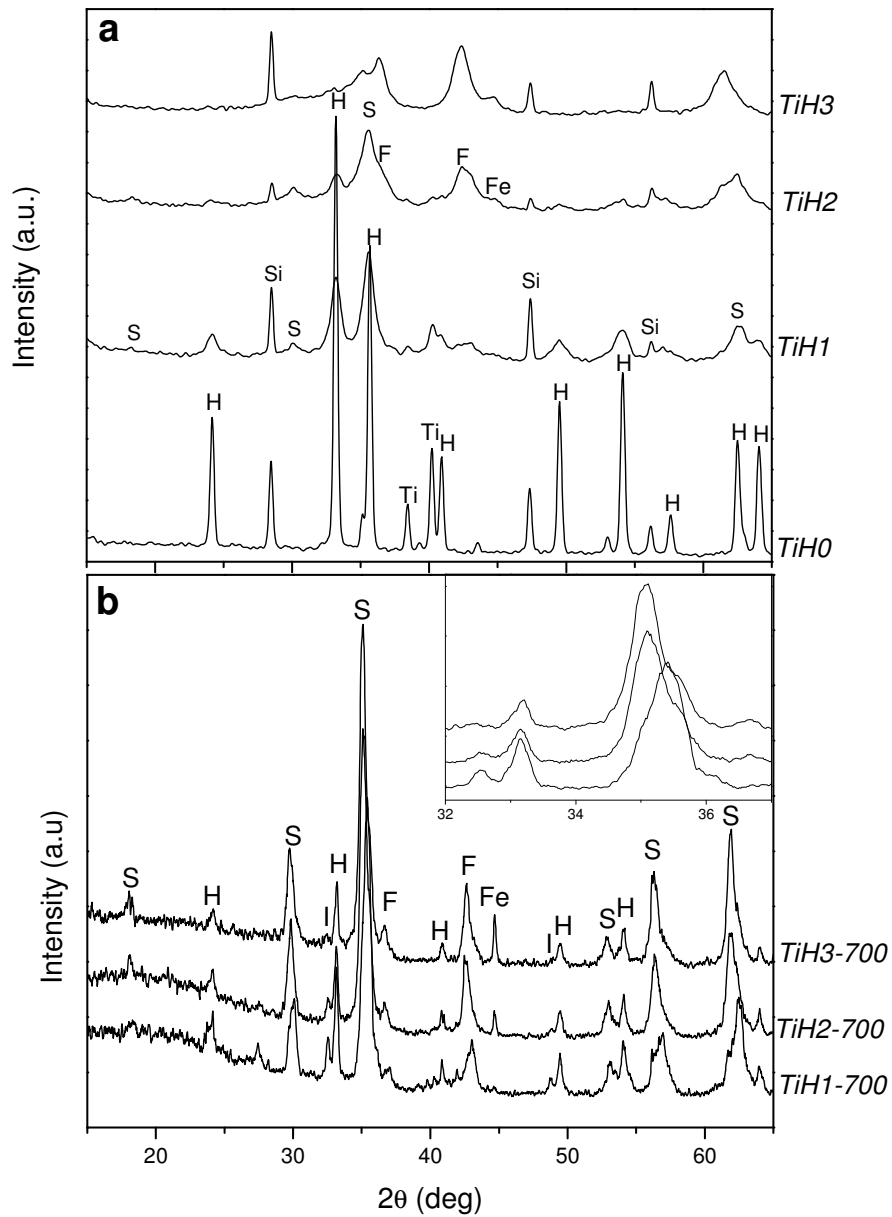


Figure 1. XRD patterns for as-milled (a) and milled and heated samples (b). F: FeO – TiO, Fe: α -iron, H: hematite, I: Ilmenite, Ti: titanium, S: solid solution ($\text{Fe}_{3-x}\text{Ti}_x\text{O}_4$), Si: silicon (added as internal reference).

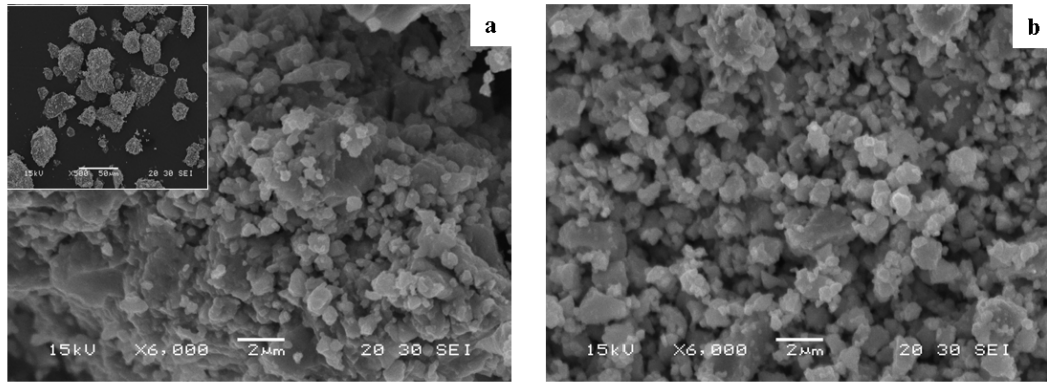


Figure 2. SEM micrographs of sample TiH₃: as milled (a) and heat-treated at 700°C (b). The inset in Fig. 2a shows a lower magnification of the main image.

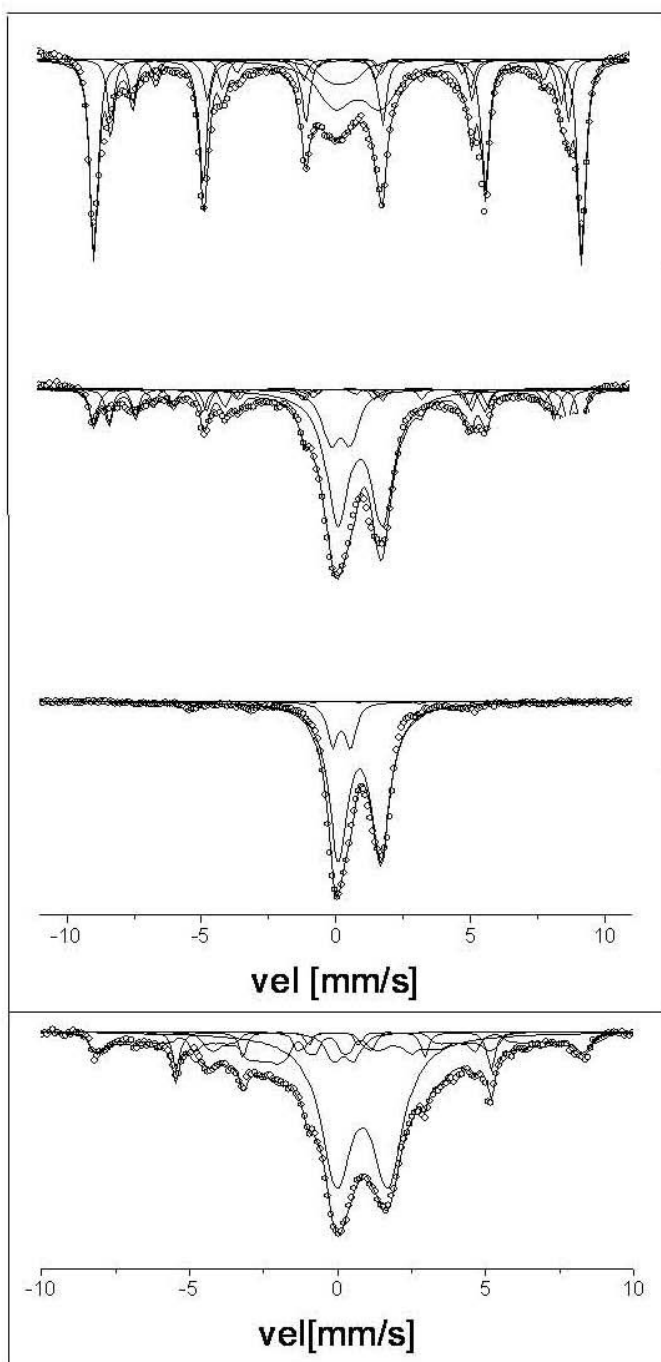


Figure 3. Room temperature Mössbauer spectra. From top to bottom: TiH1, TiH2, TiH3 and TiH3-700.

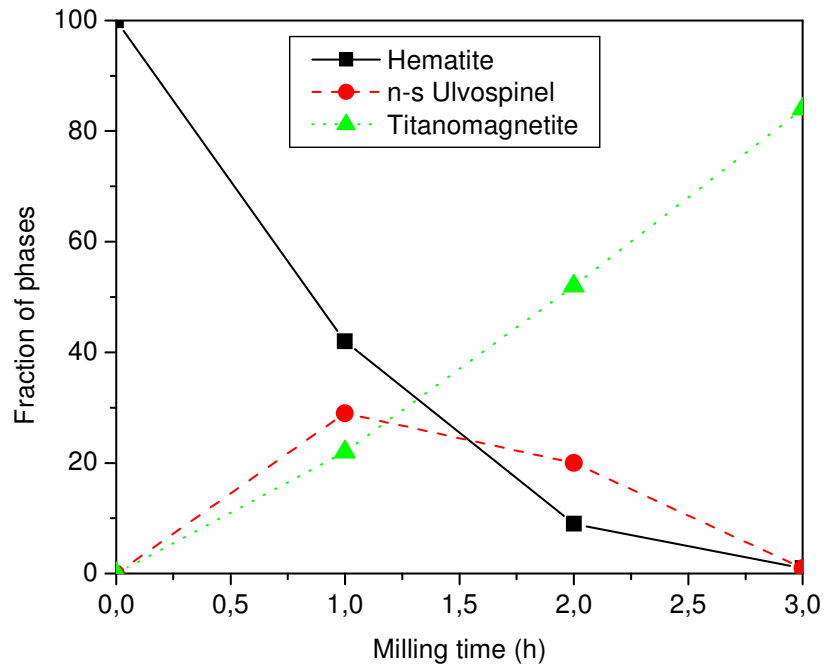


Figure 4. Evolution of the weight fractions of the non-metallic Fe-bearing phases as a function of milling time for samples TiHx (dot-lines are only a guide to the eye).

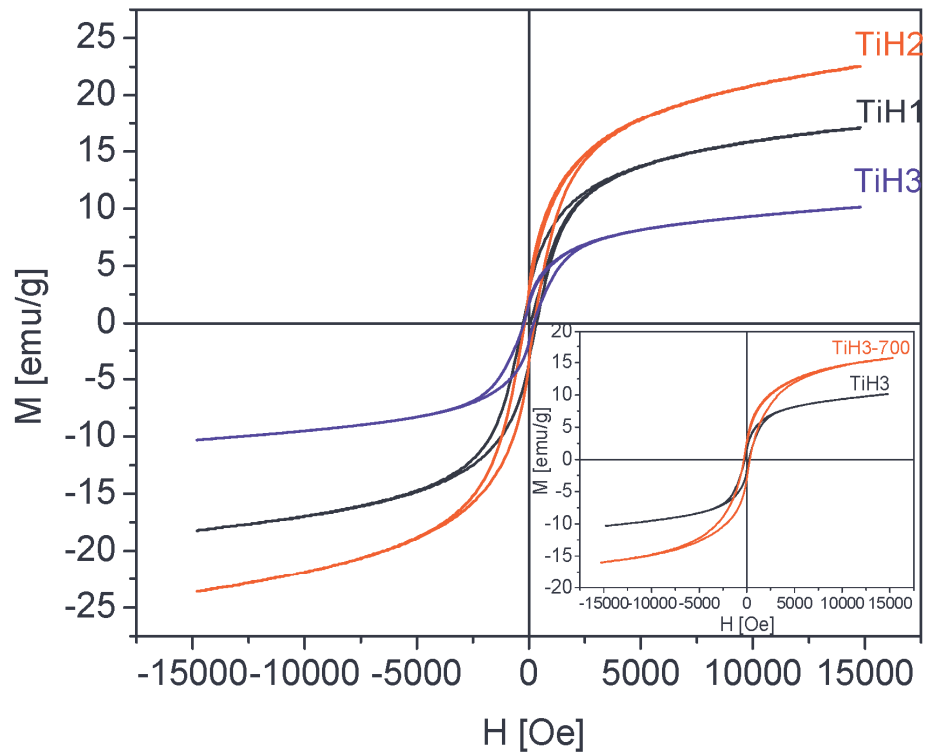


Figure 5. Hysteresis loops of the as-milled samples. The inset shows the corresponding curves of TiH3 and TiH3-700.

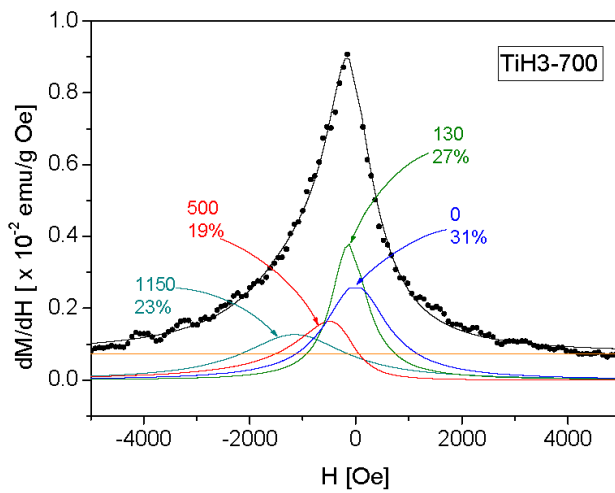
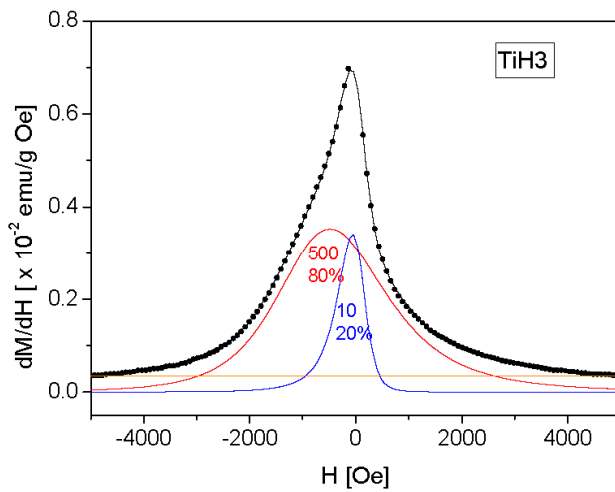
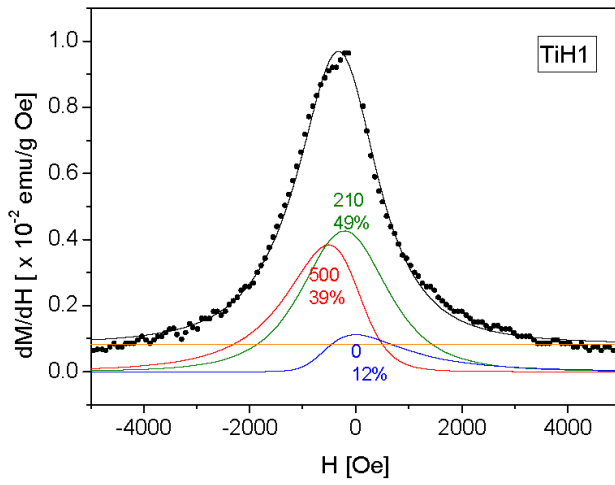


Figure 6. Susceptibility of samples TiH1, TiH3 and TiH3-700, from top to bottom, respectively. Dots are measured values and solid lines correspond to the fitting. The numbers next to each curve indicate the absolute value of the maximum of each peak.